Am J Cancer Res 2021;11(2):458-478
www.ajcr.us /ISSN:2156-6976/ajcr0121029

Original Article

IL-6 derived from therapy-induced senescence facilitates the glycolytic phenotype in glioblastoma cells

Jiayu Gu[1,2,3*], Jingyi Wang[1*], Xincheng Liu[1*], Ke Sai[4,5], Jialuo Mai[1], Fan Xing[1], Zhijie Chen[4], Xiaozhi Yang[1], Wanjun Lu[1], Cui Guo[1], Wenfeng Liu[1], Yang Xu[1], Shouxia Xie[2,3], Cheng Hu[1], Guangmei Yan[1], Wenbo Zhu[1]

[1]Department of Pharmacology, Zhongshan School of Medicine, Sun Yat-sen University, Guangzhou, China; [2]Department of Pharmacy, Shenzhen People's Hospital, The Second Clinical Medical College, Jinan University, Jinan, China; [3]The First Affiliated Hospital, Southern University of Science and Technology Shenzhen, China; [4]Department of Neurosurgery/Neuro-oncology, Sun Yat-sen University Cancer Center, Guangzhou, China; [5]State Key Laboratory of Oncology in South China, Collaborative Innovation Center for Cancer Medicine, Sun Yat-sen University Cancer Center, Guangzhou, China. [*]Equal contributors.

Received August 24, 2020; Accepted November 9, 2020; Epub February 1, 2021; Published February 15, 2021

Abstract: Activation of the cyclic adenosine monophosphate (cAMP) pathway induces the glial differentiation of glioblastoma (GBM) cells, but the fate of differentiated cells remains poorly understood. Transcriptome analyses have revealed significant changes in the cell cycle- and senescence-related pathways in differentiated GBM cells induced by dibutyryl cAMP (dbcAMP). Further investigations showed that reactive oxygen species (ROS) derived from enhanced mitochondrial function are involved in senescence induction and proliferation inhibition. Moreover, we found that IL-6 from dbcAMP- or temozolomide (TMZ)-induced senescent cells facilitates the glycolytic phenotype of GBM cells and that inhibiting the IL-6-related pathway hinders the proglycolytic effect of either agent. In patient-derived GBM xenograft models, a specific antibody targeting the IL-6 receptor tocilizumab (TCZ) significantly prolongs the survival time of TMZ-treated mice. Taken together, these results suggest that both the differentiation-inducing agent dbcAMP and the chemotherapy drug TMZ are able to drive GBM cells to senescence, and the latter releases IL-6 to potentiate glycolysis, suggesting that IL-6 is a target for adjuvant chemotherapy in GBM treatment.

Keywords: Glioblastoma, senescence, IL-6, glycolysis

Introduction

Glioblastoma (GBM) is the most common type of malignant glioma, accounting for the majority of gliomas (56.6%), with an annual incidence of 3.21 per 100,000 population and a prevalence rate of 9.23 per 100,000 population in the United States [1]. GBM is characterized by a high degree of malignancy, abundant pathophysiological angiogenesis and typical invasive growth. Although standard treatments include surgical excision, radiation therapy and temozolomide (TMZ), the five-year survival rate of GBM is only 5.6% [1]. Therefore, efforts to develop new therapies for the treatment of malignant glioma are ongoing.

Senescence is characterized by stable cell cycle arrest induced at the end of the cellular lifespan or in response to various intrinsic and extrinsic insults. It is divided into three types: oncogene-induced senescence (OIS) [2], developmental and programmed senescence (DPS) and therapy-induced senescence (TIS) [3, 4]. Recently, the therapeutic potential of p53 reactivation [5, 6] and the inhibition of c-MYC or cyclin-dependent kinase (CDK) inhibitors for cancer treatment has been ascribed to cellular senescence [7-9]. Some antineoplastic modalities, have been proven to invoke senescence [4]. These studies provoked considerable interest in TIS as an alternative therapy for cancer treatment.

TIS acts as a double-edged sword in cancer, promoting or opposing cancer initiation and progression [10]. The dark side of TIS is ascribed to the specific senescence-associated secretory phenotype (SASP), which comprises cytokines, growth factors, extracellular matrix (ECM)

components and ECM-degrading enzymes [11]. Accumulating evidence supports the notion that the SASP provides an immunosuppressive, inflammatory and catabolic microenvironment, thus stimulating tumor growth and metastasis [12, 13]. The effects of the SASP on cell proliferation and tumor growth depend on diverse genetic background. A better understanding of the SASP in different contexts in GBM will provide Perceptiveness into the evolution of powerful strategies to cellular senescence regulation will be provided with a better understanding of the SASP in different contexts in GBM.

Our research group previously certified that the cyclic adenosine monophosphate (cAMP)/PKA pathway activation enhanced mitochondrial biogenesis and transformed the metabolic pattern of GBM cells from aerobic glycolysis into oxidative phosphorylation [14]. In this cellular model, we sought to elucidate the fate of GBM cells undergoing differentiation and the underlying mechanism. We also demonstrated senescence as a response to TMZ and explored how to conquer the dark side of the SASP to improve the efficacy of TMZ.

Methods and materials

Cell culture

In PRIM-1640 medium (Gibco, Thermo Fisher Scientific, Waltham, MA, USA) and MEM (Gibco, Thermo Fisher Scientific), at the condition of 37°C under 5% CO_2, we maintained DBTRG and U87 cells respectively, supplemented with 10% FBS (Gibco, Thermo Fisher Scientific) and penicillin/streptomycin (HyClone, General Electric Healthcare Life Sciences, Boston, MA, USA). We acquired DBTRG and U87 cells from the American Type Culture Collection (ATCC, Manassas, VA, USA).

Patient-derived GBM tissue was cut into small pieces of 2-4 mm. Fat, fibrous and necrotic areas of the tumor sample were removed. The tissue pieces were transferred into a gentleMACS C Tube (Miltenyi Biotec, Bergisch Gladbach, Germany) containing the enzyme mixture and attached upside down to the sleeve of a gentleMACS Dissociator (Miltenyi Biotec). We incubated the samples at 37°C under continuous rotation with MACSmix Tube Rotator (Miltenyi Biotec). The cell suspension was applied to a MACS SmartStrainer (Miltenyi Biotec) and centrifuged at 300 g for 7 min. Finally, primary GBM single-cell suspensions should be maintained in DMEM/F12 (Gibco, Thermo Fisher Scientific) immediately for downstream applications.

Reagents

Dibutyryl cAMP (dbcAMP, Sigma-Aldrich, St. Louis, MO, USA), luteolin (Selleck Chemicals, Houston, TX, USA), N-acetyl-cysteine (NAC, Sigma-Aldrich), antimycin (Abcam, Cambridge Biomedical Campus, Cambridge, UK), BP-1-102 (Selleck Chemicals), NVP-BSK805 (Selleck Chemicals) and tocilizumab (TCZ, Actemra, 20 mg/mL, Roche, Basel, Switzerland).

Gene annotation and functional enrichment analysis

Downstream transcriptome analysis were conducted by GeneSet Enrichment Analysis (GSEA) [15], the relevant gene sets can be found in the official website of MSIGDB [16]. All parameters are set in accordance with the software recommended parameters. In the results, the gene sets with both *P* and FDR values less than 0.05 were considered to be significantly different gene sets [17].

Transcriptome data processing and analysis

Raw reads were generated by the BGISEQ-500 platform [18]. Then the gene quantification were through the recommended transcriptome analysis pipeline [19]. Genes with less than two reads per million were removed, and 13 333 genes were included for further analysis. Gene count normalization and differential expression analysis were performed using the DESeq2 package [20].

5-Ethynyl-2'-deoxyuridine (EdU) incorporation assay

According to the Click-iT® EdU Flow Cytometry Assay Kit (Invitrogen, Thermo Fisher Scientific) manual, we added 10 μM EdU to the culture medium and mixed well, After 4 hours' incubation, the medium was aspirated, and 100 μl of Click-iT® fixative and 1X Click-iT® saponin-based permeabilization were added. Finally, we incubated samples with Click-iT® reaction cocktail and DAPI (Invitrogen, Thermo Fisher Scientific) for 30 min at 25°C, protected from

light. The cells were analyzed with CytoFLEX flow cytometer (Beckman Coulter, Indianapolis, IN, USA).

Senescence-associated β-galactosidase (SA-β-gal) staining

According to the instructions of SA-β-gal Staining Kit (Cell Signaling Technology, Danvers, MA, USA), cells were washed with PBS and then fixed with fixation solution for 15 min at 25°C. After rinsing with PBS at least twice, cells were stained with β-gal staining solution and incubated at 37°C overnight in a dry incubator (without CO_2). Under a light microscope (Nikon ECLIPSE Ti-U, Tokyo, Japan), blue granules within the cytoplasm are considered positive for β-gal staining, suggesting senescence of the observed cells.

Senescence in tumor tissue was assessed in tissue cryosections preserved in optimal cutting temperature compound (OCT) freezing medium using the SA-β-gal Staining Kit (Cell Signaling Technology). Briefly, tissues were fixed with PBS containing 2% formaldehyde and 0.2% glutaraldehyde at 25°C for 5 min, washed three times with PBS and incubated for 18 h at 37°C with staining solution containing X-gal. Sections were counterstained with nuclear fast red for 20 min.

Western blot analysis

We ran sodium dodecylsulphate polyacrylamide gel electrophoresis (SDS-PAGE) of lysed cells. After the separation, the proteins were transferred from the gel to the PVDF membrane (Roche, Switzerland). Once on the membrane antibodies, primary antibodies can be used to probe for the presence of target protein because of the specifically binding of antigen with antibody. The primary antibodies, as follows: p16 (Abcam), p21 (Cell Signaling Technology), CDK2 (proteintech, IL, USA), CyclinE (EMD Millipore, MA, USA), CDK4 (Cell Signaling Technology), CDK6 (Cell Signaling Technology), cyclin D1 (Cell Signaling Technology), pRb (Cell Signaling Technology), Rb (Cell Signaling Technology), tri-methyl-histone H3 (H3K9me3, Cell Signaling), histone H2AX (Abcam), DEC1 (Abcam), β-actin (Cell Signaling Technology), and HMGB1 (Cell Signaling Technology), were added at appropriate dilution in 10 ml 0.5% blocking buffer.

Cell metabolism measurement

The basal oxygen consumption rate (OCR) and extracellular acidification rate (ECAR) were measured with a Seahorse XF Cell Mito Stress Test Kit (Agilent Technologies,) and a Seahorse XF Glycolytic Rate Assay Kit (Agilent Technologies), respectively referred to established method [14]. We plated 1.5×10^5-2.5×10^5 cells in the XF Cell Culture Microplate using PRIM-1640 medium or MEM. The day before measurements, a sensor cartridge was hydrated in XF Calibrant at 37°C in a non-CO_2 incubator overnight. The next day, we changed growth medium to assay medium from microplate and incubated for 1 hour in a 37°C non-CO_2 incubator. The sensor cartridge was loaded with compounds which were diluted in assay medium for desired concentration. Next, we placed the calibration plate with the loaded sensor cartridge on the instrument tray. After 30 mins' calibration, the cell culture microplate was loaded.

Reactive oxygen species (ROS) level analysis

Intracellular ROS generation was detected with CellROX® Oxidative Stress Reagent (Invitrogen, Thermo Fisher Scientific). Cells were removed of culture medium and labeled with 5 μM CellROX dye at 37°C for 30 min, followed by CytoFLEX flow cytometer

Mitochondrial ROS levels were detected with MitoSOX Red Mitochondrial Superoxide Indicator (Invitrogen, Thermo Fisher Scientific), which were highly selective detection of superoxide and ROS of mitochondria in living cell. Cells were stained with 5 μM MitoSOX reagent at 37°C for 10 min and analyzed by flow cytometer. The results were quantitatively performed with the mean fluorescence intensity (MFI).

Cell colony formation assay

Approximately 200 cells were plated into six-well cell culture dishes and incubated in PRIM-1640 medium or MEM containing 10% serum. After two to three weeks, macroscopic colonies were formed. We fixed cell clones with 4% paraformaldehyde solution at 25°C for 20 min. Finally, 1% crystal violet staining solution (Beyotime, Shanghai, China) were used to incubate the clones.

Real-time quantitative PCR (RT-qPCR)

TRIzol reagent (Invitrogen, Thermo Fisher Scientific) was used to extract total RNA. 2 μg RNA was reverse transcribed to cDNA with Oligo (dT) (synthesized by Invitrogen, Thermo Fisher Scientific) and Revert Aid Reverse Transcriptase (Thermo Scientific, Thermo Fisher Scientific). We used Applied Biosystem 7500 Fast Real-Time PCR system (Applied Biosystems, Thermo Fisher Scientific). The sequences of the primers used are as follows: IL-6 forward: ACTCACCTCTTCAGAACGAATTG; IL-6 reverse: CCATCTTTGGAAGGTTCAGGTTG; nDNA-B3M forward: CTGTCTCCATGTTTGATGTATCT; and nDNA-B3M reverse: TCTCTGCTCCCCACCTCTAAGT. The expression of specific genes was calculated by the comparative cycle threshold method using SuperReal PreMix SYBR Green (TIANGEN, Beijing, China).

Enzyme-linked immunosorbent assay (ELISA)

IL-6 was measured with an ELISA (Invitrogen, Thermo Fisher Scientific). To determine the IL-6 levels secreted from dbcAMP-treated GBM cells, 50 μL of either the standard or cellular supernatant sample was added to each well of the ELISA plate. Fifty microliters of biotin conjugate was added to each well, and the wells were covered with an adhesive film. Microwell strips were incubated at room temperature (18 to 25°C) for 2 h with shaking at 400 rpm. After washing the microwell strips 4 times, 100 μL of streptavidin-HRP was added to each well and incubated at room temperature (18 to 25°C) for 1 h with shaking at 400 rpm. After washing the microwell strips, 50 μL of TMB substrate solution followed by 50 μL of stopping buffer were added to each well, and absorption was measured at 450 nm.

Xenograft GBM animal models

10^5 GSCs were subcutaneously inoculated on 4-week-old female BALB/c-nu/nu mice. After tumors were developed to about 50 mm^3, all the mice were intraperitoneally treated with vehicle, dbcAMP plus luteolin (dL group), TMZ, TCZ, dL plus TCZ, or TMZ plus TCZ. dbcAMP was intraperitoneally administered at a dosage of 20 mg/kg/day, and luteolin was intraperitoneally administered at a dosage of 40 mg/kg/day. TMZ was intraperitoneally administered at a dosage of 50 mg/kg/day for the first 5 days. TCZ was intravenously injected at a dosage of 100 mg/kg/week. Length and width of tumors were measured with the caliper, followed computational formula: length × $width^2/2$ = volume (mm^3). Data are shown as the mean ± SD.

5×10^4 GSCs were injected into the skull of BALB/c-nu/nu mice to perform the orthotopic GBM model. After 3 days, we divided them randomly into six groups as described above. The mice were monitored daily, and the survival state was recorded.

Immunohistochemical analysis

According to the established method [14], Slides were incubated with a primary antibody against Ki-67 overnight at 4°C. Then, the cells were incubated with an HRP-conjugated secondary antibody at 25°C. Positive expression cells were counted under a light microscope.

Statistical analysis

All statistical analyses were performed using GraphPad Prism 7.0. For the in vitro studies, difference between two groups was calculated with an unpaired Student's t test, and differences between more than two groups were calculated with analysis of variance (ANOVA). Differences in body weight were calculated with repeated measures ANOVA. Differences in survival were calculated with Kaplan-Meier analysis. The points on the curves indicate glioma-related deaths (*P* values were determined by log-rank analysis). All error bars indicate the SD. Differences were considered significant if the *P* value was less than 0.05.

Results

Transcriptome analyses reveal the senescence pattern in GBM cells treated with the differentiation-inducing agent dbcAMP

As reported previously, activation of the cAMP signaling pathway can induce the differentiation of human GBM cells toward the astrocyte type [14]. In this study, we aimed to determine the fate of GBM cells following cAMP-induced differentiation. We assessed the effect of dbcAMP treatment on the global gene expression pattern of the human GBM cell lines DBTRG and U87 using RNA sequencing (RNA-Seq) analysis. By performing a gene set enrich-

ment analysis (GSEA) of the transcriptome data, we observed that the gene sets associated with astrocyte or neuron differentiation in DBTRG and U87 cells were significantly upregulated by dbcAMP treatment, while the gene sets associated with oligodendrocyte differentiation were downregulated (**Figure 1A**). These results support the previous finding that activation of the cAMP pathway induces the neural differentiation of GBM cells. We further determined the top 10 most enriched pathways in these two cell lines (**Figure 1B**), of which the cell cycle and cellular senescence ranked in the top 3. Moreover, the heatmaps of the gene sets revealed that dramatic downregulation of the cell cycle-related gene set occurred at 48 hours in both cell lines (**Figure 1C**), while the senescence-related gene set was characterized by the downregulation of proliferation-related genes and the upregulation of cytokine- and apoptosis-related genes. These data indicate that the exposure of GBM cells to dbcAMP may induce cell cycle arrest and senescence concurrent with differentiation.

dbcAMP induces the senescence of cultured GBM cell lines and primary cultured GBM cells

Based on the significant changes in the cell cycle pathway in the transcriptome analysis with dbcAMP treatment, we first assessed the proliferation capacity of dbcAMP-treated glioma cells with an EdU incorporation assay. As shown in **Figure 2A** and **2B**, the percentage of EdU-positive DBTRG cells in control group was 28.12%, while in the dbcAMP-treated 4 days group at was 0.49%. Similarly, the percentage of EdU-positive U87 cells decreased from 25.91% to 0.25% after dbcAMP treatment for 4 days.

Then, we tested the senescence phenotype characterized by SA-β-gal activity [21] and a series of biomarkers, including increased trimethylation at Lys9 of histone 3 (H3K9me3) [22, 23], enhanced expression of the DNA damage marker γ-H2AX (a phosphorylated form of the histone variant H2AX) [24, 25], enhanced differentiation of embryo-chondrocyte expressed gene 1 (DEC1) [26] and decreased nuclear localization of high mobility group protein B1 (HMGB1) [27]. As shown in **Figure 2C-E**, dbcAMP treatment triggered the typical senescence phenotype of DBTRG and U87 cells.

The canonical signaling pathways that induce senescence include p16 (cyclin-dependent kinase inhibitor 2A, CDKN2A)-dependent pathways and p21 (cyclin-dependent kinase inhibitor 1, CDKN1A)-dependent pathways. The activation of p16 and p21 respectively inhibits the CDK4/6-cyclin D1 and CDK2-cyclin E complexes, thus resulting in a decrease in Rb phosphorylation and ultimately senescence [28, 29].

Here, as **Figure 2F** shown, western blotting revealed that the protein levels of p16 were increased and those of p21, CDK4/6 and cyclin D1 were decreased following dbcAMP treatment in both GBM cell lines. CDK2 and cyclin E were decreased in DBTRG cells while increased in U87 cells after dbcAMP treatment. Rb works as the checkpoint of G1/S phase, the phosphorylated level of which determines the released level of E2F and promotes cells going from G1 into S phase. In DBTRG and U87 cells, phosphorylated Rb (pRb) was remarkably decreased. Taken these together, the increase in p16 and the decrease in CDK4/6-cyclin D1 and CDK2-cyclin E complex may contribute to the pRb decrease in DBTRG cells, while only the alteration of p16 and CDK4/6-cyclin D1 complex involves in the pRb decrease in U87 cells.

We then evaluated TIS in patient-derived primary cultured GBM cells. After dbcAMP treatment, primary cultured GBM cells also underwent senescence, as evidenced by the increased level of SA-β-gal (**Figure 2G**).

ROS derived from enhanced mitochondrial function account for senescence induction and proliferation inhibition by dbcAMP

We previously demonstrated that dbcAMP drives glial differentiation by enhancing mitochondrial biogenesis and oxidative phosphorylation [14]. Enhanced oxidative phosphorylation is evidenced by an increase in the basal and maximal OCR, as shown in **Figure 3A**. Given that ROS, as toxic byproducts of the mitochondrial respiratory chain, tend to contribute to DNA damage, senescence, or cell death, it is reasonable to hypothesize that dbcAMP-induced senescence is attributed to ROS derived from enhanced mitochondrial respiratory activity. dbcAMP-induced cells were loaded with CellROX® Reagen, which indicates intracellular total ROS levels (**Figure 3B**), and MitoSOX Red, which indicates mitochondrial-derived ROS lev-

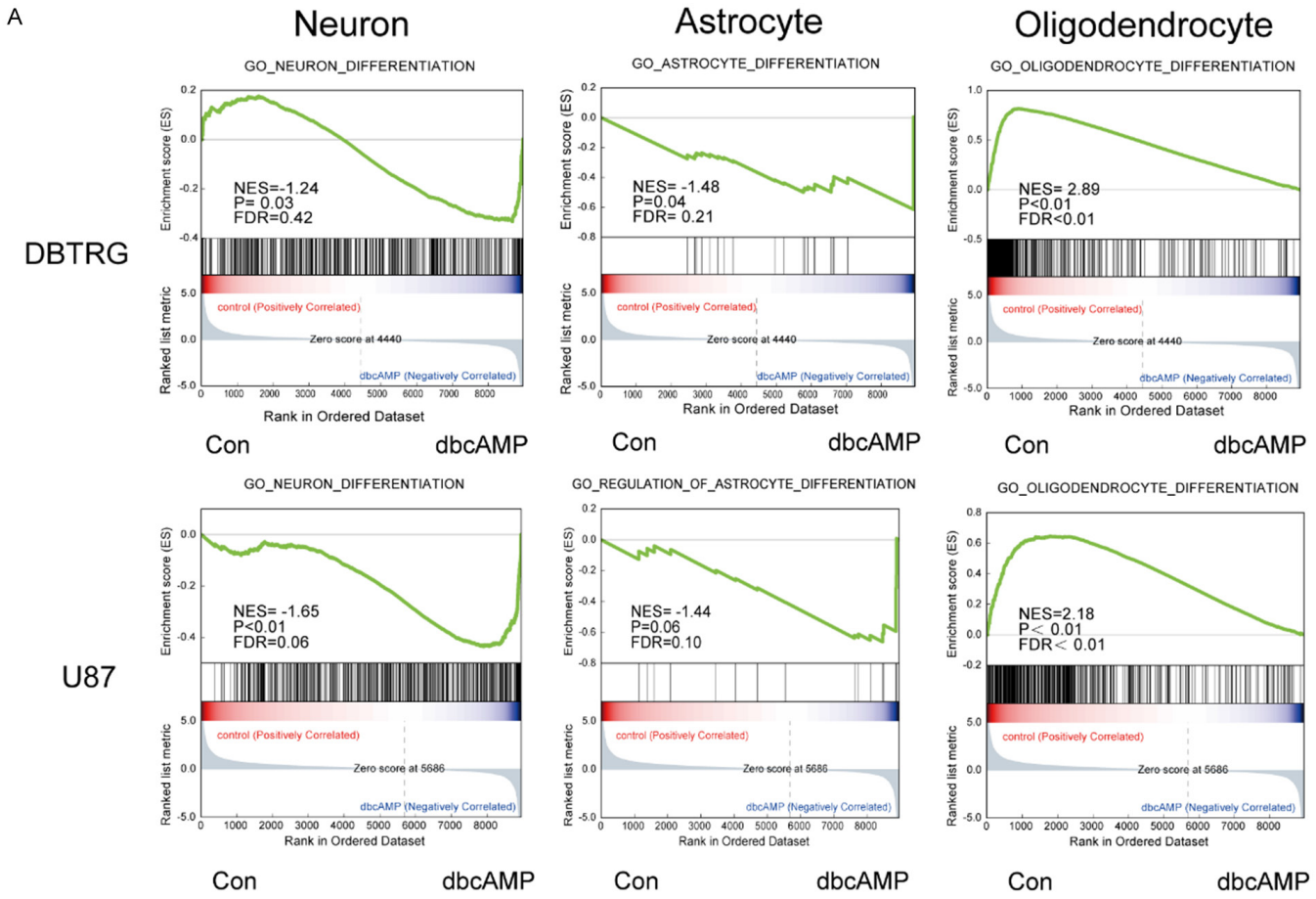
A
Neuron
Astrocyte
Oligodendrocyte
DBTRG
U87
GO_NEURON_DIFFERENTIATION
GO_ASTROCYTE_DIFFERENTIATION
GO_OLIGODENDROCYTE_DIFFERENTIATION
GO_NEURON_DIFFERENTIATION
GO_REGULATION_OF_ASTROCYTE_DIFFERENTIATION
GO_OLIGODENDROCYTE_DIFFERENTIATION
NES=-1.24
P= 0.03
FDR=0.42
NES= -1.48
P=0.04
FDR= 0.21
NES= 2.89
P<0.01
FDR<0.01
NES= -1.65
P<0.01
FDR=0.06
NES= -1.44
P=0.06
FDR=0.10
NES=2.18
P< 0.01
FDR< 0.01
Enrichment score (ES)
Ranked list metric
control (Positively Correlated)
dbcAMP (Negatively Correlated)
Zero score at 4440
Zero score at 5686
Rank in Ordered Dataset
Con
dbcAMP

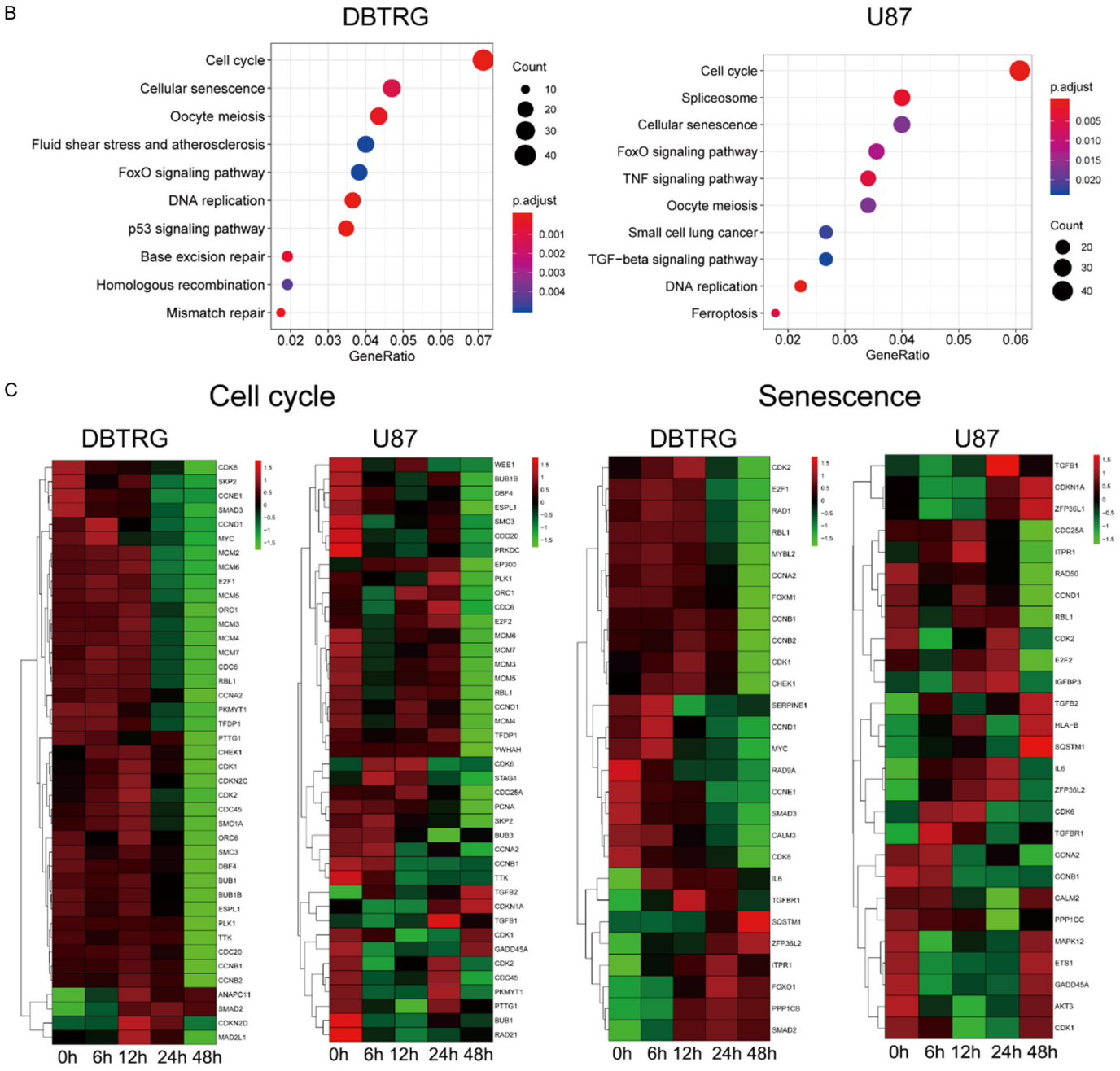
B
DBTRG
Cell cycle
Cellular senescence
Oocyte meiosis
Fluid shear stress and atherosclerosis
FoxO signaling pathway
DNA replication
p53 signaling pathway
Base excision repair
Homologous recombination
Mismatch repair
0.02 0.03 0.04 0.05 0.06 0.07
GeneRatio
Count
10
20
30
40
p.adjust
0.001
0.002
0.003
0.004
U87
Cell cycle
Spliceosome
Cellular senescence
FoxO signaling pathway
TNF signaling pathway
Oocyte meiosis
Small cell lung cancer
TGF−beta signaling pathway
DNA replication
Ferroptosis
0.02 0.03 0.04 0.05 0.06
GeneRatio
p.adjust
0.005
0.010
0.015
0.020
Count
20
30
40
C
Cell cycle
Senescence
DBTRG
U87
DBTRG
U87
0h 6h 12h 24h 48h
0h 6h 12h 24h 48h
0h 6h 12h 24h 48h
0h 6h 12h 24h 48h

Figure 1. Transcriptome profiles reveal senescence and cell cycle changes in dbcAMP-treated cells. A. GSEA enrichment plots of differentiation-related genes ranked based on dbcAMP-induced differentiation. P<0.05 and FDR<0.25 indicate a statistically significant difference. NES>0 indicates that most genes were downregulated with dbcAMP treatment compared with the control. NES<0 indicates that most genes were upregulated with dbcAMP treatment compared with the control. B. Top 10 most enriched pathways in DBTRG cells. Top 10 most enriched pathways in U87 cells. Dots represent term enrichment: red indicates high enrichment, and blue indicates low enrichment. The sizes of the dots represent the percentage of each row. Normalized enrichment scores are shown in the bar chart. C. Heatmaps of the expression levels of senescence- and cell cycle-related genes. High expression is shown in red, and low expression is shown in green.

els (**Figure 3C**), and analyzed by FCM. Antimycin, an inhibitor of oxidative phosphorylation, successfully reversed ROS accumulation in DBTRG and U87 cells (**Figure 3D**), further indicating the mitochondrial derivation of ROS.

To evaluate whether ROS production is responsible for proliferation inhibition and senescence induced by dbcAMP, we pretreated cells with the ROS scavenger NAC and observed decreased ROS production (**Figure 3E**). Consistent with this finding, decreased clone formation (**Figure 3F**, **3G**), SA-β-gal (**Figure 3H**) and enhanced senescence biomarkers (**Figure 3I**) by dbcAMP treatment were reversed with NAC. These results strongly suggest that ROS account for proliferation arrest and senescence induction.

IL-6 secretion from senescent GBM cells induced by dbcAMP facilitates the glycolytic phenotype of GBM cells

Senescent cells secrete a complex mixture of ECM (uPA, tPA, MMPs, etc.) and soluble (IL-6, IL-1a, IL-1b, IL-8, GROα, MCP-1, etc.) factors; this is referred to as the SASP [11, 30]. In this study, we analyzed the dbcAMP-induced SASP in DBTRG and U87 cells and found that IL-6 was the most prominent factor (**Figure 4A**). Data from GBM patients showed that high IL-6 expression was associated with a dismal outcome (**Figure 4B**), indicating IL-6 as an independent risk factor for predicting the prognosis of GBM patients.

Next, we verified that the transcriptional expression and secretion of IL-6 were increased by dbcAMP treatment in GBM cell lines (**Figure 4C** and **4D**). The increase in IL-6 secretion can be also observed in patient-derived primary cultured GBM cells (**Figure 4E**).

IL-6, as one of the major cytokines in the tumor microenvironment, is well known for its prosurvival and proinflammatory activities. Herein, we sought to explore whether IL-6 secreted by senescent cancer cells influences the metabolic phenotype of untreated cancer cells. We collected conditioned medium (CM) from senescent cells and then incubated untreated GBM cells with the CM. As shown in **Figure 4F**, CM from dbcAMP-treated cells increased the extracellular acidification rate (ECAR) of tumor cells, indicating the pro-Warburg effect. The increase in the ECAR was reversed by inhibitors of JAK2 and STAT3 downstream of IL-6 (NVP-BSK805 and BP-1-102) (**Figure 4G** and **4H**), indicating that the pro-Warburg effect is attributed to IL-6 pathway activation.

To further clarify the glycolysis related genes regulated by IL-6/STAT3 signal activation, we performed GSEA from the RNA-seq data and found significant positive-correlated glycolysis induced by dbcAMP alongside the treatment time (**Figure 4I**). A series of glycolytic enzyme-encoding genes were significantly upregulated after dbcAMP-treatment, including hexokinase 2 (HK2), glyceraldehyde 3-phosphate dehydrogenase (GAPDH) and so on (**Figure 4J**).

In summary, we demonstrate that IL-6, secreted by senescent cells, regulates glycolysis in GBM cells through the classical downstream molecule STAT3 and may work via upregulating the expression of glycolytic enzyme-encoding genes.

IL-6 secretion from senescent GBM cells induced by TMZ facilitates the glycolytic phenotype of GBM cells

TMZ, a DNA-alkylating agent, is the first-line chemotherapeutic drug for GBM. In clinical practice, substantial resistance is frequently observed. We thus explored whether TMZ could induce cell senescence and thus potentiate glycolysis in GBM cells, which may account for therapy resistance. As shown in **Figure 5A** and **5B**, TMZ remarkably induced the senescence of DBTRG cells and the secretion of IL-6. More-

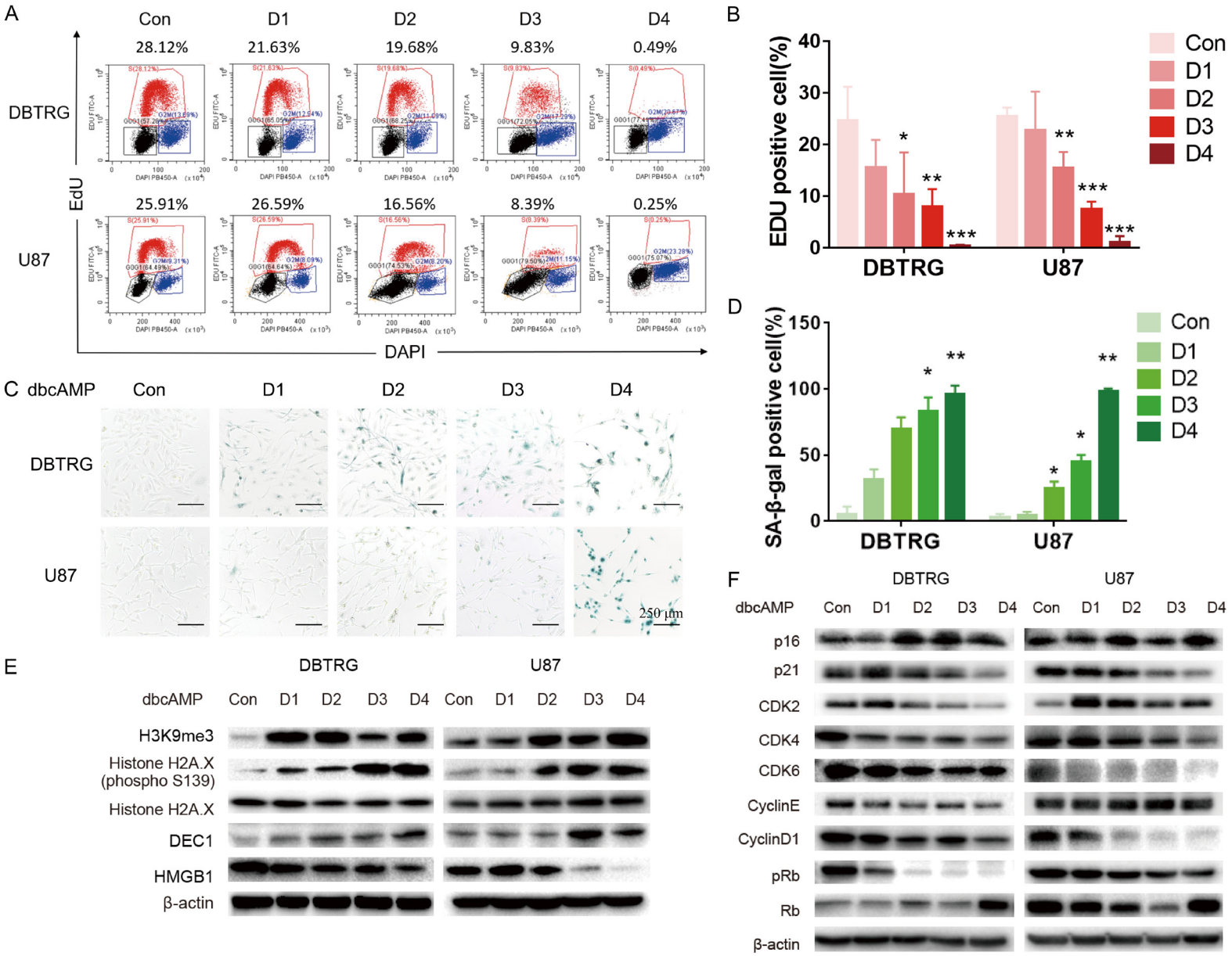
A
Con
D1
D2
D3
D4
28.12%
21.63%
19.68%
9.83%
0.49%
DBTRG
EdU
25.91%
26.59%
16.56%
8.39%
0.25%
U87
DAPI
B
EDU positive cell(%)
40
30
20
10
0
Con
D1
D2
D3
D4
DBTRG
U87
C dbcAMP
Con
D1
D2
D3
D4
DBTRG
U87
250 μm
D
SA-β-gal positive cell(%)
150
100
50
0
DBTRG
U87
E
DBTRG
U87
dbcAMP
Con
D1
D2
D3
D4
H3K9me3
Histone H2A.X (phospho S139)
Histone H2A.X
DEC1
HMGB1
β-actin
F
DBTRG
U87
dbcAMP
Con
D1
D2
D3
D4
p16
p21
CDK2
CDK4
CDK6
CyclinE
CyclinD1
pRb
Rb
β-actin

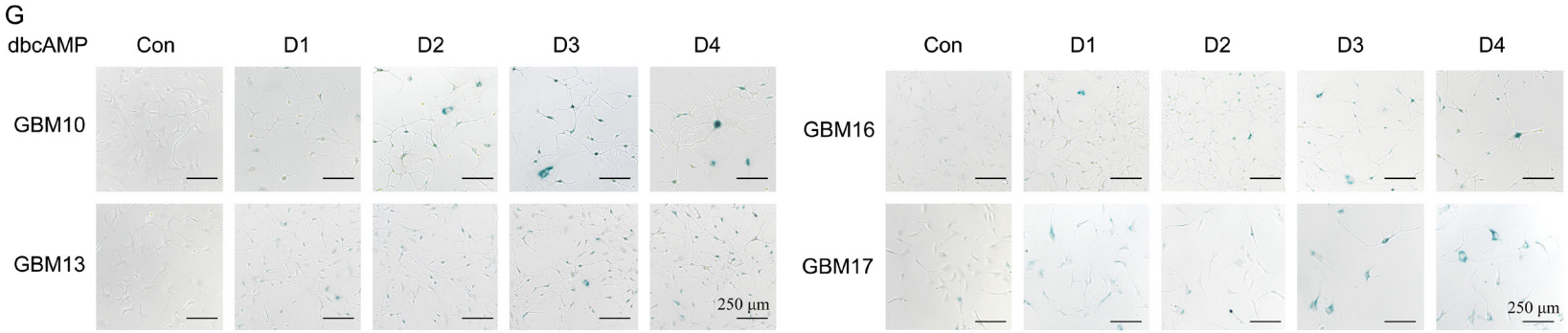

Figure 2. cAMP activation induces the senescence of cultured GBM cell lines and patient-derived GBM cells. (A, B) Proportion of EdU-positive DBTRG and U87 cells. (C) The bright-field images of β-Gal activity staining. Cells with blue staining were considered senescent. Scale bar, 250 μm. (D) The statistical data of SA-β-gal-positive cells. (E) Protein expression of senescence biomarkers, including H3K9me3, histone H2A.X (phosphorylated S139), total H2A.X, DEC1 and HMGB1, in DBTRG and U87 cells, as detected by western blot analysis. (F) Expression of proteins involved in senescence-inducing pathways, including p16, p21, CDK2, CDK4, CDK6, cyclin E, and cyclin D1, phosphorylated and total Rb in DBTRG and U87 cells, as detected by western blot analysis. (G) The bright-field images of β-Gal activity staining. Cells with blue staining were considered senescent. Scale bar, 250 μm. DBTRG cells, U87 cells and primary patient-derived GBM cells were treated with 1 mM dbcAMP for 1, 2, 3 and 4 days and then subjected to FCM (A), β-gal activity staining analysis (C and G), and western blot analysis (E and F).

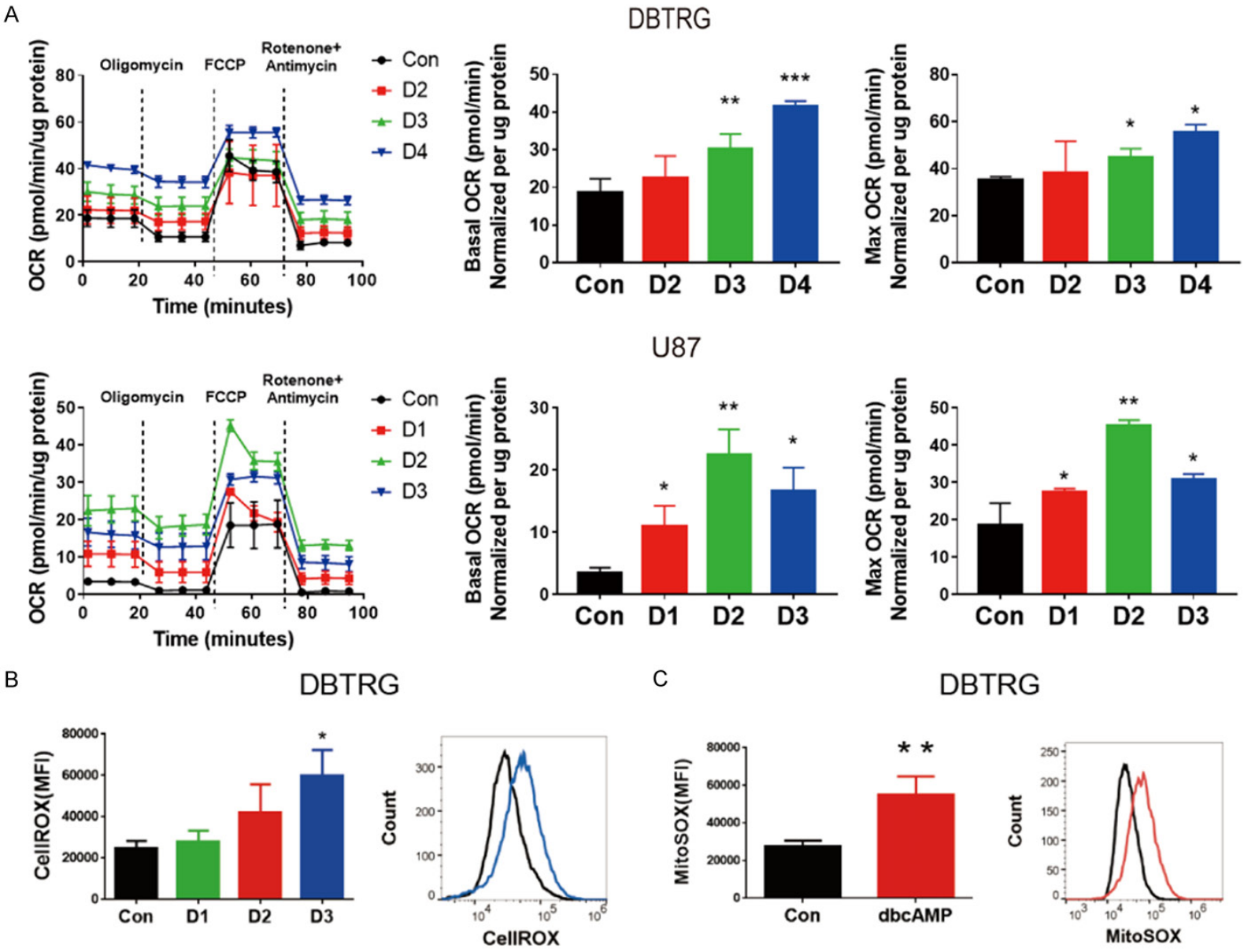
A
DBTRG
Oligomycin
FCCP
Rotenone+ Antimycin
Con
D2
D3
D4
OCR (pmol/min/ug protein)
Time (minutes)
Basal OCR (pmol/min) Normalized per ug protein
Max OCR (pmol/min) Normalized per ug protein
U87
D1
B
DBTRG
CellROX(MFI)
Count
CellROX
C
DBTRG
MitoSOX(MFI)
dbcAMP
MitoSOX

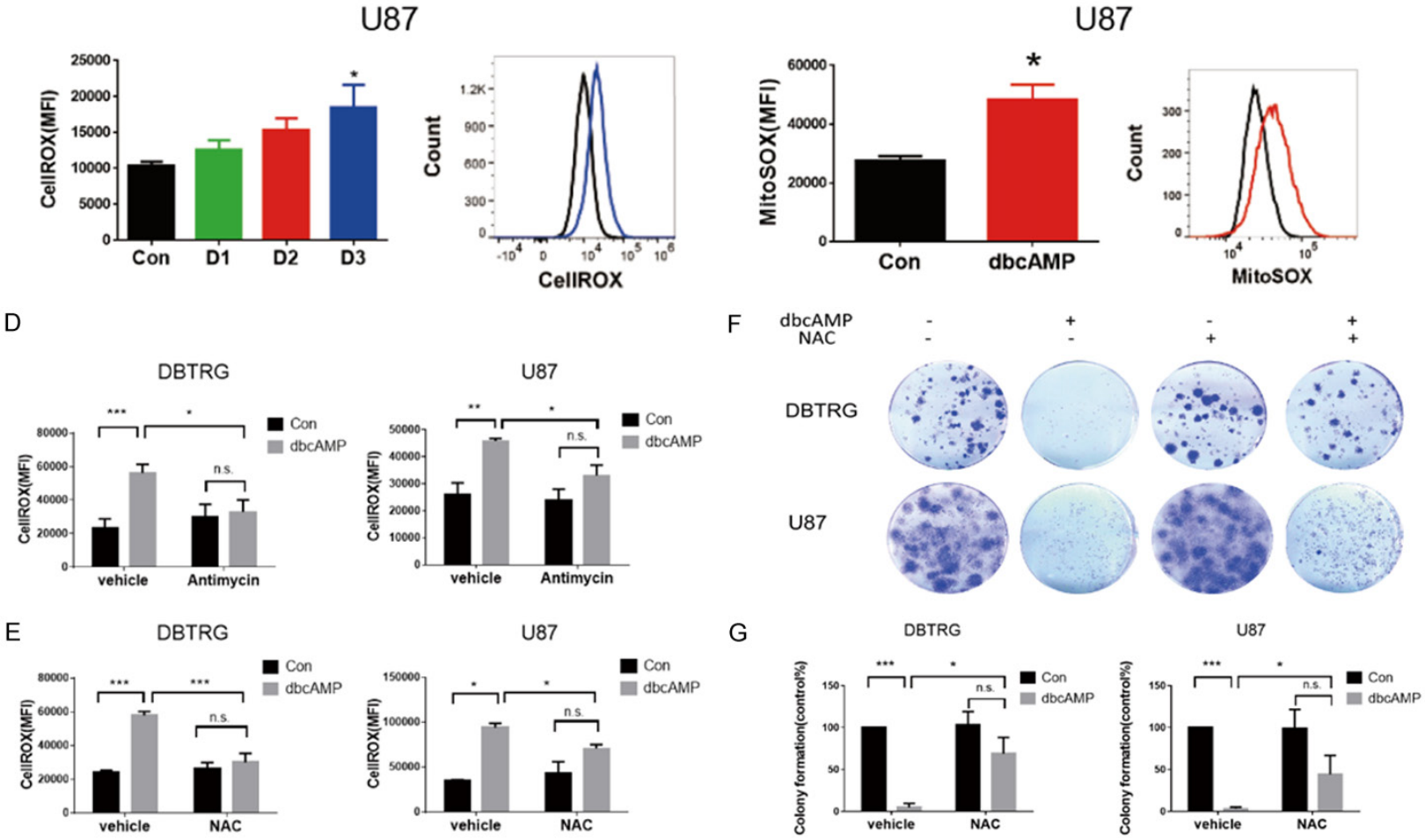
U87
CellROX(MFI)
Con
D1
D2
D3
Count
CellROX
U87
MitoSOX(MFI)
Con
dbcAMP
Count
MitoSOX
D
DBTRG
U87
CellROX(MFI)
Con
dbcAMP
vehicle
Antimycin
n.s.
F
dbcAMP
NAC
DBTRG
U87
E
DBTRG
U87
CellROX(MFI)
vehicle
NAC
n.s.
G
DBTRG
U87
Colony formation(control%)
vehicle
NAC
n.s.

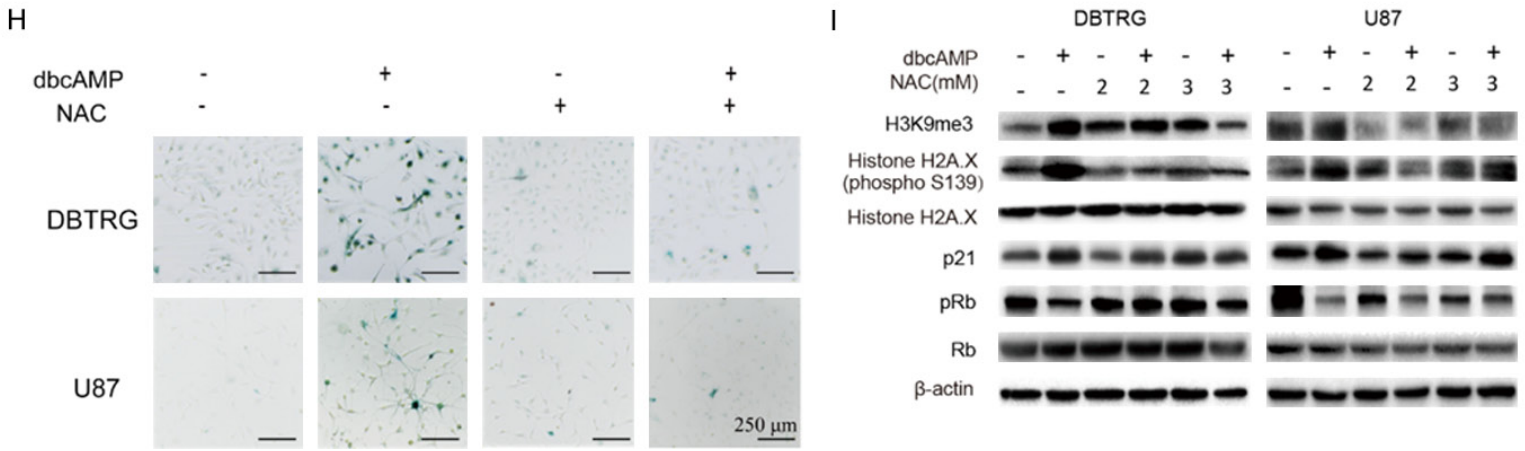

Figure 3. The accumulation of ROS derived from enhanced mitochondrial function accounts for senescence induction and proliferation inhibition by dbcAMP. (A) Time-dependent effect of dbcAMP treatment on the OCR. DBTRG Cells were treated with 1 mM dbcAMP for 2, 3 and 4 days. U87 Cells were treated with 1 mM dbcAMP for 1, 2 and 3 days. OCR were monitored with the Seahorse XFe24 Analyzer in real time. Dotted lines indicate incubation of cells with the indicated compounds. Basal and max OCR values were normalized with total protein. (B, C) dbcAMP enhanced intracellular (B) and mitochondrial (C) ROS production. Glioblastoma cells were treated with 1 mM dbcAMP for 1, 2 and 3 days. The MFI of CellROX signals, which represent total intracellular ROS level, were determined by FCM. Histogram represent the fluorescence intensity of 3 days treatment (B). MitoSOX dye was used to detect the changes of mitochondrial-derived ROS levels in glioblastoma cells after 1 mM dbcAMP treatment for 3 days (C). (D) Antimycin, as inhibitor of mitochondria respiratory chain, reversed the increased ROS level by dbcAMP. DBTRG and U87 cells were treated with or without 1 mM dbcAMP and 5 nM Antimycin for 3 days. (E-I) Effects of the ROS scavenger NAC on CellROX signals (E), clone formation (F), SA-β-gal positive staining (H) and senescence-related signaling molecules (I). (G) The statistical data of colony formation percentage. Cells were treated with 1 mM dbcAMP and/or NAC (2 or 3 mM) and then subjected to FCM (E), clone formation assays (F), SA-β-gal activity analysis (H) and western blot analysis (I).

over, CM from TMZ-induced senescent cells enhanced the glycolytic capacity of DBTRG cells as did dbcAMP, which was reversed by the STAT3 inhibitor BP-1-102 (**Figure 5C**). All these data suggest that TMZ enhances the glycolytic phenotype of GBM cells by inducing TIS, in which IL-6 plays a predominant role.

The IL-6 receptor antibody cooperates with TMZ to prolong the survival time of mice

Based on the effects of cAMP signal activators or TMZ on senescence and IL-6 secretion mentioned above, we further evaluated the antitumor activity of these two groups of agents combined with the IL-6 receptor antibody in vivo. In the GSC-derived GBM xenograft model, dbcAMP and the PDE inhibitor luteolin (dL) were used as cAMP signal activators, TMZ was used as the classic chemotherapeutic drug for GBM, and a clinical drug for rheumatoid arthritis, TCZ, was used as the IL-6 receptor antibody. The treatment schedule is shown in **Figure 6A**. As shown in **Figure 6B**, dL alone, TMZ alone and TCZ alone significantly repressed tumor growth, and the effects of dL and TMZ were much stronger than those of TCZ. However, regarding tumor size, TCZ was not synergistic with dL or TMZ. Body weight was also measured, and no difference between any group was observed, indicating the safety of each drug alone and the combination treatment (**Figure 6C**). In addition, all the treatment groups demonstrated an increase in SA-β-gal activity and a decrease in the number of Ki-67-positive cells (**Figure 6D** and **6E**), suggesting the induction of senescence and the inhibition of proliferation by the therapeutic agents in vivo. Consistent with the data showing tumor size alterations, TCZ did not potentiate the prosenescent or antiproliferative activity of dL or TMZ (**Figure 6E**).

We then used patient-derived GSCs to establish an orthotopic GBM model and administered the same regimen as in the subcutaneous xenograft model (**Figure 6F**). Notably, dL treatment significantly prolonged the survival time compared with the vehicle, while TCZ did not potentiate this effect. Intriguingly, TMZ alone did not alter the survival time of mice, while TCZ combined with TMZ markedly prolonged the survival time compared with TMZ or TCZ alone (**Figure 6G**).

In summary, the IL-6 receptor antibody TCZ does not enhance the antitumor activity of cAMP activators or TMZ in the subcutaneous GBM model, while TCZ, but not cAMP activators, significantly synergizes with TMZ to prolong the survival time of mice bearing orthotopic GBM. These data imply that the SASP, similar to IL-6, promotes tumor progression by influencing the systemic microenvironment.

Discussion

At present, GBM is a major refractory disease that remains a serious hazard to human health. Therefore, it is quite urgent to better understand its molecular biology, microenvironment effect and immune interaction with the host. The preliminary work of our research group revealed that activation of the cAMP/PKA pathway reverses the Warburg effect by facilitating the mitochondrial biogenesis and ultimately directs GBM cells to differentiate into astrocyte-like cells [14]. In this study, we found that the fate of DBTRG and U87 GBM cells undergoing differentiation by dbcAMP is senescence attributed to enhanced oxidation phosphorylation and mitochondria-derived ROS production. As with dbcAMP treatment, TMZ, the first-line drug for GBM, also induced the senescence of GBM cells. In vitro, senescent cells induced by both agents secreted IL-6, which enhances glycolysis in GBM cells. In vivo, the survival time of TMZ-treated mice was prolonged by the antibody targeting the IL-6 receptor tocilizumab (**Figure 7**). Our data strongly support that TIS potentiates the glycolysis of GBM cells via IL-6 and thus provide a scientific rationale for reversing resistance to the GBM therapeutic drug TMZ.

Senescence is one manner by which cells defend against cancer after cellular DNA repair and apoptosis and is characterized by cell cycle arrest and expression of the SA-β-gal phenotype and the SASP. TIS is currently considered a potential strategy for cancer therapy by virtue of the suppressive mechanism of tumorigenesis and subsequent clearance by immune cells [31]. In GBM cell lines and patient-derived GBM cells, we found that the differentiation-inducing agent dbcAMP is a senescence inducer. The molecular pathway that activates senescence coverage is p16, not the p21 tumor suppressor pathway. Primarily, oxidative stress induced by

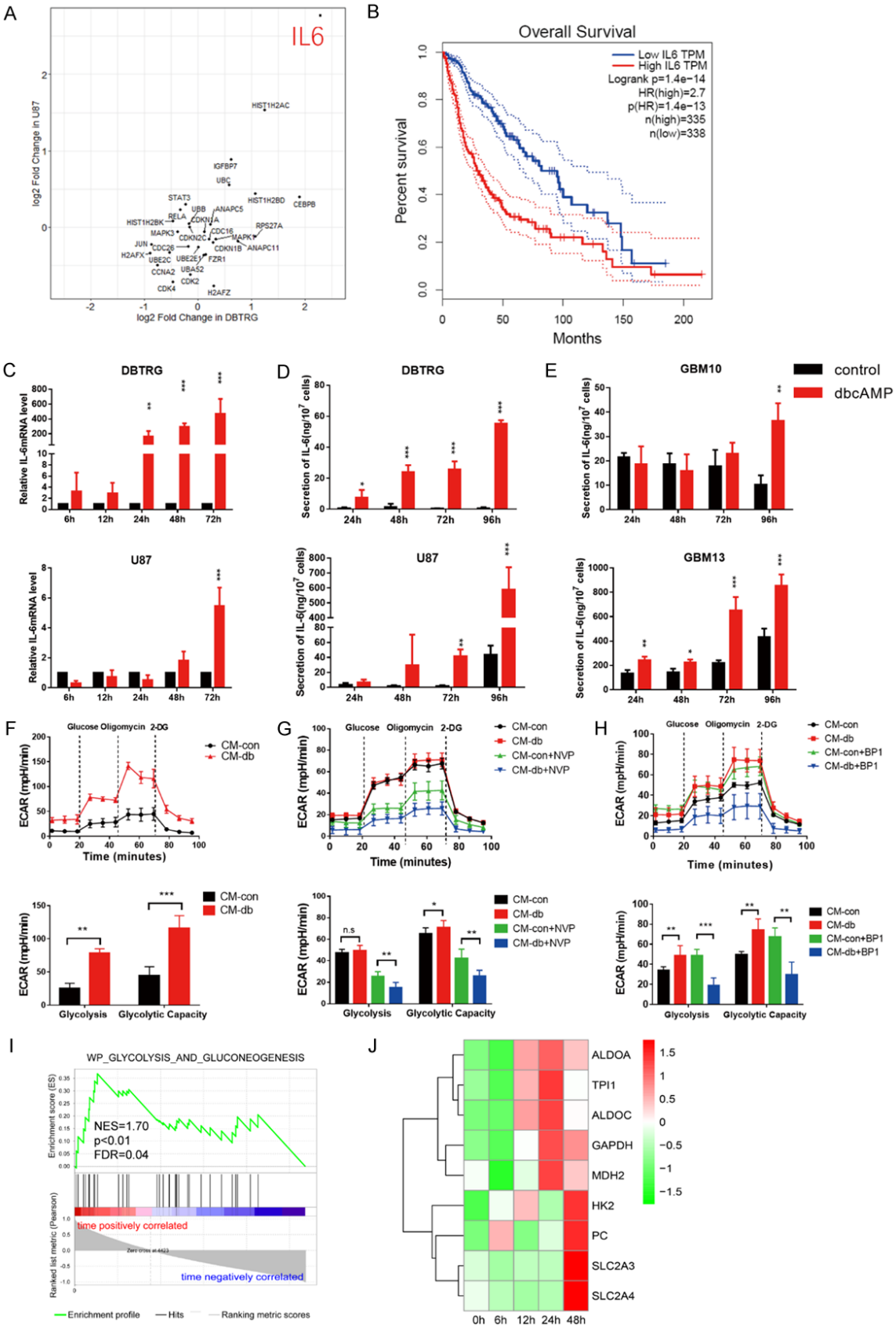
A
IL6
log2 Fold Change in U87
log2 Fold Change in DBTRG
HIST1H2AC
IGFBP7
UBC
STAT3
HIST1H2BD
CEBPB
UBB
ANAPC5
RELA
CDKN1A
HIST1H2BK
RPS27A
MAPK3
CDC16
CDKN2C
MAPK1
JUN
CDC26
CDKN1B
ANAPC11
H2AFX
UBE2C
UBE2E1
FZR1
CCNA2
UBA52
CDK2
CDK4
H2AFZ
B
Overall Survival
Low IL6 TPM
High IL6 TPM
Logrank p=1.4e−14
HR(high)=2.7
p(HR)=1.4e−13
n(high)=335
n(low)=338
Percent survival
Months
C
DBTRG
Relative IL-6mRNA level
U87
D
DBTRG
Secretion of IL-6(ng/10^7 cells)
U87
E
GBM10
GBM13
control
dbcAMP
F
Glucose Oligomycin 2-DG
CM-con
CM-db
ECAR (mpH/min)
Time (minutes)
Glycolysis
Glycolytic Capacity
G
CM-con
CM-db
CM-con+NVP
CM-db+NVP
n.s
H
CM-con
CM-db
CM-con+BP1
CM-db+BP1
I
WP_GLYCOLYSIS_AND_GLUCONEOGENESIS
Enrichment score (ES)
NES=1.70
p<0.01
FDR=0.04
Ranked list metric (Pearson)
time positively correlated
time negatively correlated
Enrichment profile
Hits
Ranking metric scores
J
ALDOA
TPI1
ALDOC
GAPDH
MDH2
HK2
PC
SLC2A3
SLC2A4
0h 6h 12h 24h 48h

Figure 4. The cAMP-induced SASP factor IL-6 facilitates the glycolytic phenotype of GBM cells. (A) A volcano plot of differentially expressed transcripts between control and dbcAMP-treated DBTRG and U87 cells. The arrow indicates the differentially expressed IL-6 gene. (B) IL-6 mRNA expression and overall survival were analyzed in glioma and GBM patients. Data were obtained from The Cancer Genome Atlas (TCGA) database and analyzed by cBioPortal for Cancer Genomics. (C) Relative mRNA levels of IL-6 by real-time qPCR in DBTRG and U87 cells treated with db-cAMP (1 mM) for 6, 12, 24, 48 and 72 hours. (D and E) IL-6 protein levels secreted by DBTRG and U87 cells (D) or patient-derived primary GBM cells (E) treated with dbcAMP (1 mM) for 24, 48, 72 and 96 hours, as determined by ELISAs. (F) Effects of conditioned medium from dbcAMP-treated cells (CMdb) for 3 days on the ECAR. The ECAR was monitored by using the Seahorse XFe24 Analyzer in real time. (G) Effects of the JAK2 inhibitor NVP-BSK805 (5 μM) on the increased ECAR induced by CMdb. (H) Effects of the STAT3 inhibitor BP-1-102 (5 μM) on the increased ECAR induced by CMdb. In (F-H), DBTRG cells were pretreated with or without NVP-BSK805 or BP-1-102 for 1 day and then co-incubated with CMdb for an additional 2 days. (I) GSEA analysis of glycolysis gene sets. Results with P<0.05, FDR<0.25 represents that the difference was statistically significant. NES>0, represents that pathway was directly proportional to the treatment time of dbcAMP. (J) Heatmap of the glycolysis related genes in the U87 cells. The gene expression of U87 cells treated with 1 mM dbcAMP at 0, 6, 12, 24, 48 hours were plotted. The expression abundance of each gene was scaled among five time point.

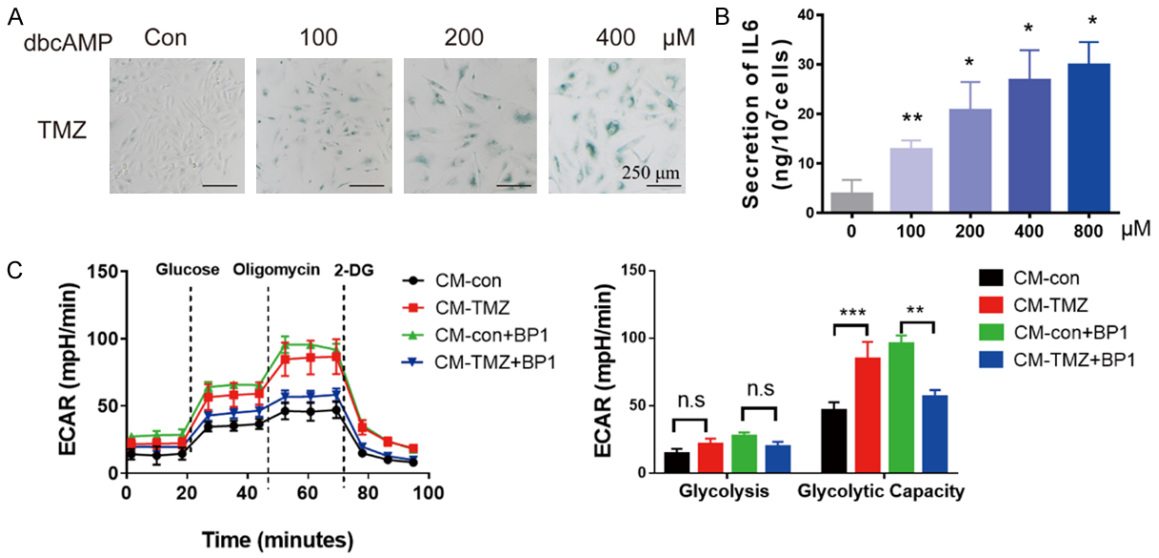

Figure 5. The TMZ-induced SASP factor IL-6 facilitates the glycolytic phenotype of GBM cells. A. Effects of TMZ on SA-β-gal activity in DBTRG cells. DBTRG cells were treated with 100, 200, 400 μM TMZ for 7 days and then stained with SA-β-gal. Cells with blue staining were considered senescent. Scale bar, 250 μm. B. IL-6 protein levels secreted by DBTRG cells with or without TMZ, as determined by ELISAs. C. Effects of CM-TMZ and/or BP-1-102 (5 μM) on the ECAR in DBTRG cells. DBTRG cells were pretreated with or without BP-1-102 for 1 day and then coincubated with CM-TMZ for an additional 2 days. The ECAR was monitored by using the Seahorse XFe24 Analyzer in real time.

dbcAMP activates these key tumor suppressor pathways, leading to cell cycle arrest, followed by senescence. The chemotherapy agent TMZ was found to induce the senescence of GBM cells, consistent with the result showing p21-dependent senescence in glioma cells [32]. These data provide senescence induction as a rational mechanism underlying the anti-GBM activity of cAMP activators and TMZ.

Based on different microenvironments and genetic backgrounds, senescence tends to behave as a double-edged sword owing to the complexity of the SASP [13]. In one aspect, the SASP can reinforce the growth arrest of senescent cells and facilitate the recruitment of immune cells to remove senescent cells. In the other aspect, some SASP factors support tumor vascularization and induce epithelial-mesenchymal transition and cancer cell invasion. Thus, senescence induction may provide a new explanation for the drug resistance commonly observed in TMZ therapy. To effectively overcome this weakness, it is crucial to determine the factors that contribute to the dark side of senescence. In our study, we found that one SASP factor (i.e., IL-6) was present at a high level in dbcAMP- and TMZ-induced senescent

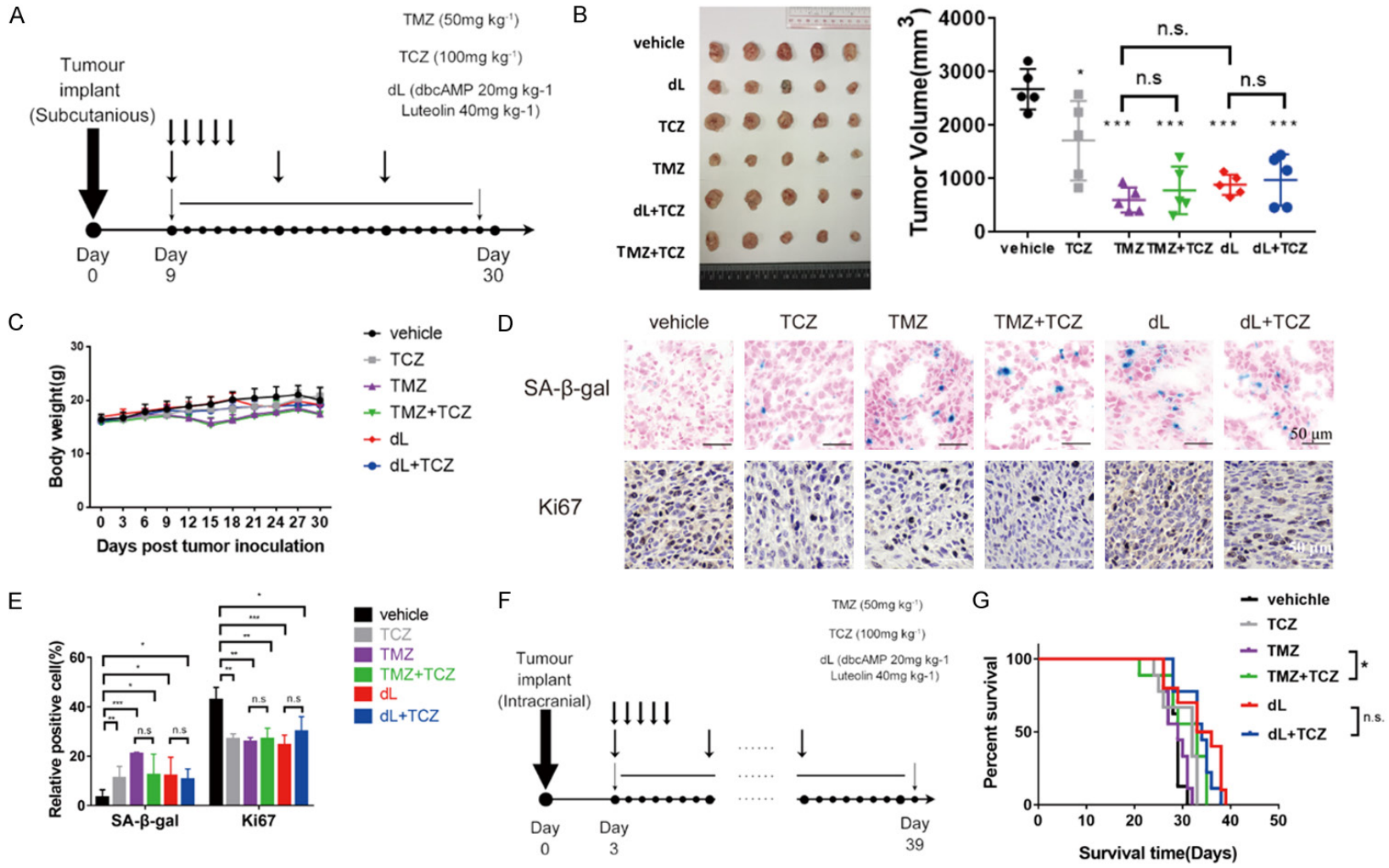

Figure 6. Therapy-induced tumor growth inhibition and senescence in GBM xenograft models and TMZ plus the IL-6 receptor antibody prolong the survival time of mice. A. The schematic drawing of treatment regimen in xenograft model. Nu/nu mice were subcutaneously inoculated with patient-derived GSCs. Nine days after inoculation, mice were grouped into vehicle, dbcAMP plus luteolin (dL), TMZ, TCZ, dL plus TCZ and TMZ plus TCZ groups (n=5 mice/group). dbcAMP was intraperitoneally administered at a dosage of 20 mg/kg/day for 21 days, and luteolin was intraperitoneally administered at a dosage of 40 mg/kg/day for 21 days. TMZ was intraperitoneally administered at a dosage of 50 mg/kg/day for the first 5 days. TCZ was intravenously injected at a dosage of 100 mg/kg/week for a total of 3 doses. B and C. Tumor images and tumor volume statistics were obtained from mice after sacrifice, and the body weights of the mice were monitored every 3 days. D and E. Images and statistical data of SA-β-gal-activated and Ki-67-positive cells. Tumor tissues were evaluated by SA-β-gal activity analysis and immunohistochemistry for Ki-67. Scale bar, 50 μm. F. The schematic drawing of treatment regimen in orthotopic model. Nu/nu mice were intracranially inoculated with GSCs. Three

days after inoculation, mice were grouped into vehicle (n=8 mice/group), dL (n=10), TMZ (n=9), TCZ (n=9), dL plus TCZ (n=9) and TMZ plus TCZ (n=9) groups. dbcAMP was intraperitoneally administered at a dosage of 20 mg/kg/day until the occurrence of death, and luteolin was intraperitoneally administered at a dosage of 40 mg/kg/day until the occurrence of death. TMZ was intraperitoneally administered at a dosage of 50 mg/kg/day for the first 5 days. TCZ was intravenously injected at a dosage of 100 mg/kg/week until the occurrence of death. G. Antitumor activity in the orthotopic GBM model. Survival curve and Kaplan-Meier an alyses were conducted.

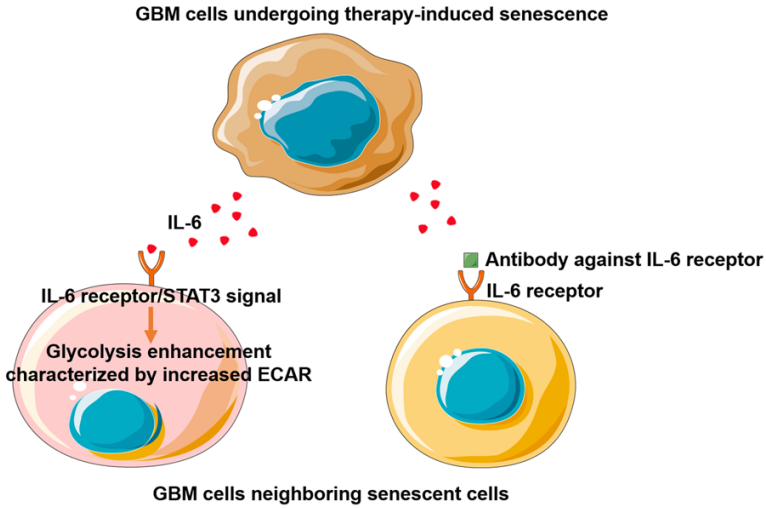

Figure 7. A schematic model. Therapy-induced senescent cells secreted IL-6, which activates IL-6 receptor/STAT3 signal and then enhances glycolysis characterized by increased ECAR in GBM cells. Neutralization of IL-6 receptor can hamper the glycolysis enhancement induced by IL-6.

cells. Inhibitors targeting JAK2 and STAT3 downstream of IL-6 reversed the proglycolytic activity of CM from dbcAMP- and TMZ-treated GBM cells, indicating that IL-6 can enforce tumorigenesis in an autocrine and/or paracrine manner. In an animal model, TMZ combined with the IL-6 receptor antibody tocilizumab prolonged the survival time of mice bearing intracranial GBM compared with TMZ alone, further supporting the dark role of IL-6 in the cancer microenvironment and the potential for targeting the IL-6 signaling pathway as a TMZ synergist.

IL-6 is a well-studied molecule that is identified as an inflammatory cytokine, a proliferation-promoting factor and an angiogenesis factor. It is highly expressed in several cancers, such as colorectal cancer, breast cancer, prostate cancer, ovarian carcinoma, pancreatic cancer, lung cancer, and renal cell carcinoma, which are associated with aggressive tumor growth and response to therapies [33]. Through data mining, we found that a high level of IL-6 in GBM, is associated with a poor prognosis, consistent with data on other cancer types. In addition, we found that elevated levels of IL-6 contribute to the glycolytic phenotype in GBM cells, in agreement with data showing the glycolysis-stimulating activity induced by the IL-6/GP130/STAT3 signaling pathway in pancreatic cancer [34] and data showing elevated glucose consumption and lactate production by IL-6 treatment in GBM cells [35]. These results support persistent IL-6 signaling as a viable therapeutic target for GBM using IL-6 signal inhibitors.

By mining the RNA-sequencing data in U87 cells, we find that the gene cluster of glycolysis was significantly upregulated, including some key glycolytic enzymes such as hexokinase 2 (HK2) and glyceraldehyde 3-phosphate dehydrogenase (GAPDH). But it is needed to further elucidate if these genes are directly controlled by STAT3. In human multiple myeloma cells, we also mine the transcriptome data (GSE115558) [36], and find that the transcriptional expression of these two enzymes were also positively related with IL-6, in consistent of the result in U87 cells. These facts demonstrate that the IL-6 acts on transcription factor STAT3 and then might upregulate the expression of glycolytic enzymes accounting for the pro-glycolysis effect.

In this study, we observed seemingly inconsistent results between the subcutaneous GBM model and the intracranial model. In the subcutaneous GBM model, the IL-6 receptor antibody tocilizumab did not cooperate with TMZ to induce a stronger effect on diminishing tumor size. However, in the intracranial model, tocilizumab plus TMZ significantly prolonged the survival time compared with tocilizumab or TMZ. These results suggest that IL-6 promotes tumorigenesis not by directly stimulating cell growth but by influencing systemic metabolism

in GBM. In addition, we demonstrated that tocilizumab did not improve the survival time of mice treated with dbcAMP plus luteolin. We speculate that there are other factors involved in cAMP-induced senescence in addition to IL-6 that contribute significantly.

Kirkland and Tchkonia found that the FDA-approved chemotherapy drug dasatinib eliminated senescent human fat cell progenitors, while the plant-derived health-food supplement quercetin was more effective against senescent human endothelial cells and mouse bone marrow mesenchymal stem cells (BM-MSCs) [37]. A recent study demonstrated that a series of small molecular compounds, such as BCL-2 family inhibitors, could kill senescent hematopoietic stem cells [38]. As a result, the clearance of senescent glial cells can prevent tau-dependent pathology and cognitive decline [39], and the clearance of senescent cells seemed to extend the lifespan of normally aging mice by delaying tumorigenesis and improving the age-related deterioration of several organs, including the kidney, heart and fat [40]. These results demonstrate the possibility of adding specific agents targeting senescent cells on the basis of senescence inducers for the treatment of cancer and other aging-related diseases. In the future, the combination of differentiation inducers and/or traditional chemotherapeutics with senescence scavengers could be developed into a strategy for maximizing antitumor effects.

In summary, our data suggest that ROS derived from enhanced oxidative phosphorylation mediate cAMP-induced cell cycle arrest and senescence. Furthermore, we show that IL-6 is a key SASP factor secreted from therapy-induced GBM senescent cells that mediates glycolysis enhancement by CM from senescent cells. Targeting IL-6 abrogates the enhanced glycolysis-promoting activity in vitro and prolongs the survival time in combination with TMZ in vivo, thus providing a novel target for improving the prognosis of GBM patients with TMZ treatment.

Acknowledgements

We acknowledge our laboratory members for assistance and helpful discussion. This work was supported by the National Natural Science Foundation of China (No. 81872886, 81872887, 81802536 and 81773751), Natural Science Foundation of Guangdong Province (No. 2017A030313620), the National Major Scientific, Technological Special Project for "Significant New Drugs Development" during the 13th Five-Year Plan Period (No. 2018ZX09733002), Pioneering talents project of Guangzhou Development Zone, Guangdong Province (No. CY2018-012) and Shenzhen Key Medical Discipline Construction Fund (No. SZXK059). We are grateful to Professor Zhongping Chen, principal of Department of Neurosurgery and Neuro-oncology, Sun Yat-sen University Cancer Center, State Key Laboratory of Oncology in South China, and Collaborative Innovation Center for Cancer Medicine, for providing patient-derived primary glioblastoma (GBM) cells for our research.

Disclosure of conflict of interest

None.

Address correspondence to: Dr. Wenbo Zhu, Department of Pharmacology, Zhongshan School of Medicine, Sun Yat-sen University, 74 Zhongshan Road 2, Guangzhou 510080, Guangdong Province, China. Tel: +86-2087333258; Fax: +86-02087330578; E-mail: zhuwenbo@mail.sysu.edu.cn

References

[1] Ostrom QT, Gittleman H, Truitt G, Boscia A, Kruchko C and Barnholtz-Sloan JS. CBTRUS statistical report: primary brain and other central nervous system tumors diagnosed in the United States in 2011-2015. Neuro Oncol 2018; 20: iv1-iv86.

[2] Acosta JC and Gil J. Senescence: a new weapon for cancer therapy. Trends Cell Biol 2012; 22: 211-219.

[3] von Kobbe C. Cellular senescence: a view throughout organismal life. Cell Mol Life Sci 2018; 75: 3553-3567.

[4] Perez-Mancera PA, Young AR and Narita M. Inside and out: the activities of senescence in cancer. Nat Rev Cancer 2014; 14: 547-558.

[5] Ventura A, Kirsch DG, McLaughlin ME, Tuveson DA, Grimm J, Lintault L, Newman J, Reczek EE, Weissleder R and Jacks T. Restoration of p53 function leads to tumour regression in vivo. Nature 2007; 445: 661-665.

[6] Xue W, Zender L, Miething C, Dickins RA, Hernando E, Krizhanovsky V, Cordon-Cardo C and Lowe SW. Senescence and tumour clearance is triggered by p53 restoration in murine liver carcinomas. Nature 2007; 445: 656-660.

[7] Lee S and Schmitt CA. The dynamic nature of senescence in cancer. Nat Cell Biol 2019; 21: 94-101.
[8] Schmitt CA, Fridman JS, Yang M, Lee S, Baranov E, Hoffman RM and Lowe SW. A senescence program controlled by p53 and p16INK4a contributes to the outcome of cancer therapy. Cell 2002; 109: 335-346.
[9] Lee CS, Baek J and Han SY. The role of kinase modulators in cellular senescence for use in cancer treatment. Molecules 2017; 22: 1411.
[10] Frey N, Venturelli S, Zender L and Bitzer M. Cellular senescence in gastrointestinal diseases: from pathogenesis to therapeutics. Nat Rev Gastroenterol Hepatol 2018; 15: 81-95.
[11] Ovadya Y and Krizhanovsky V. Senescent cells: SASPected drivers of age-related pathologies. Biogerontology 2014; 15: 627-642.
[12] Mavrogonatou E, Pratsinis H and Kletsas D. The role of senescence in cancer development. Semin Cancer Biol 2020; 62: 182-191.
[13] Faget DV, Ren Q and Stewart SA. Unmasking senescence: context-dependent effects of SASP in cancer. Nat Rev Cancer 2019; 19: 439-453.
[14] Xing F, Luan Y, Cai J, Wu S, Mai J, Gu J, Zhang H, Li K, Lin Y, Xiao X, Liang J, Li Y, Chen W, Tan Y, Sheng L, Lu B, Lu W, Gao M, Qiu P, Su X, Yin W, Hu J, Chen Z, Sai K, Wang J, Chen F, Chen Y, Zhu S, Liu D, Cheng S, Xie Z, Zhu W and Yan G. The anti-warburg effect elicited by the cAMP-PGC1alpha pathway drives differentiation of glioblastoma cells into astrocytes. Cell Rep 2017; 18: 468-481.
[15] Liberzon A, Subramanian A, Pinchback R, Thorvaldsdottir H, Tamayo P and Mesirov JP. Molecular signatures database (MSigDB) 3.0. Bioinformatics 2011; 27: 1739-1740.
[16] Subramanian A, Tamayo P, Mootha VK, Mukherjee S, Ebert BL, Gillette MA, Paulovich A, Pomeroy SL, Golub TR, Lander ES and Mesirov JP. Gene set enrichment analysis: a knowledge-based approach for interpreting genome-wide expression profiles. Proc Natl Acad Sci U S A 2005; 102: 15545-15550.
[17] Reimand J, Isserlin R, Voisin V, Kucera M, Tannus-Lopes C, Rostamianfar A, Wadi L, Meyer M, Wong J, Xu C, Merico D and Bader GD. Pathway enrichment analysis and visualization of omics data using g: profiler, GSEA, Cytoscape and EnrichmentMap. Nat Protoc 2019; 14: 482-517.
[18] Huang J, Liang X, Xuan Y, Geng C, Li Y, Lu H, Qu S, Mei X, Chen H, Yu T, Sun N, Rao J, Wang J, Zhang W, Chen Y, Liao S, Jiang H, Liu X, Yang Z, Mu F and Gao S. A reference human genome dataset of the BGISEQ-500 sequencer. Gigascience 2017; 6: 1-9.
[19] Robertson G, Schein J, Chiu R, Corbett R, Field M, Jackman SD, Mungall K, Lee S, Okada HM, Qian JQ, Griffith M, Raymond A, Thiessen N, Cezard T, Butterfield YS, Newsome R, Chan SK, She R, Varhol R, Kamoh B, Prabhu AL, Tam A, Zhao Y, Moore RA, Hirst M, Marra MA, Jones SJ, Hoodless PA and Birol I. De novo assembly and analysis of RNA-seq data. Nat Methods 2010; 7: 909-912.
[20] Love MI, Huber W and Anders S. Moderated estimation of fold change and dispersion for RNA-seq data with DESeq2. Genome Biol 2014; 15: 550.
[21] Schosserer M, Grillari J and Breitenbach M. The dual role of cellular senescence in developing tumors and their response to cancer therapy. Front Oncol 2017; 7: 278.
[22] Adams PD. Remodeling of chromatin structure in senescent cells and its potential impact on tumor suppression and aging. Gene 2007; 397: 84-93.
[23] Narita M, Nunez S, Heard E, Narita M, Lin AW, Hearn SA, Spector DL, Hannon GJ and Lowe SW. Rb-mediated heterochromatin formation and silencing of E2F target genes during cellular senescence. Cell 2003; 113: 703-716.
[24] Hewitt G, Jurk D, Marques FDM, Correia-Melo C, Hardy T, Gackowska A, Anderson R, Taschuk M, Mann J and Passos JF. Telomeres are favoured targets of a persistent DNA damage response in ageing and stress-induced senescence. Nature Communications 2012; 3: 708.
[25] Fumagalli M, Rossiello F, Clerici M, Barozzi S, Cittaro D, Kaplunov JM, Bucci G, Dobreva M, Matti V, Beausejour CM, Herbig U, Longhese MP and d'Adda di Fagagna F. Telomeric DNA damage is irreparable and causes persistent DNA-damage-response activation. Nat Cell Biol 2012; 14: 355-365.
[26] Qian Y, Zhang J, Yan B and Chen X. DEC1, a basic helix-loop-helix transcription factor and a novel target gene of the p53 family, mediates p53-dependent premature senescence. J Biol Chem 2008; 283: 2896-2905.
[27] Davalos AR, Kawahara M, Malhotra GK, Schaum N, Huang J, Ved U, Beausejour CM, Coppe JP, Rodier F and Campisi J. p53-dependent release of Alarmin HMGB1 is a central mediator of senescent phenotypes. J Cell Biol 2013; 201: 613-629.
[28] Lowe SW, Cepero E and Evan G. Intrinsic tumour suppression. Nature 2004; 432: 307-315.
[29] Smits VA, Klompmaker R, Vallenius T, Rijksen G, Makela TP and Medema RH. p21 inhibits Thr161 phosphorylation of Cdc2 to enforce the G2 DNA damage checkpoint. J Biol Chem 2000; 275: 30638-30643.

[30] Coppe JP, Desprez PY, Krtolica A and Campisi J. The senescence-associated secretory phenotype: the dark side of tumor suppression. Annu Rev Pathol 2010; 5: 99-118.
[31] Lee S and Lee JS. Cellular senescence: a promising strategy for cancer therapy. BMB Rep 2019; 52: 35-41.
[32] Aasland D, Gotzinger L, Hauck L, Berte N, Meyer J, Effenberger M, Schneider S, Reuber EE, Roos WP, Tomicic MT, Kaina B and Christmann M. Temozolomide induces senescence and repression of DNA repair pathways in glioblastoma cells via activation of ATR-CHK1, p21, and NF-kappaB. Cancer Res 2019; 79: 99-113.
[33] Kumari N, Dwarakanath BS, Das A and Bhatt AN. Role of interleukin-6 in cancer progression and therapeutic resistance. Tumour Biol 2016; 37: 11553-11572.
[34] Chen X, Tian J, Su GH and Lin J. Blocking IL-6/GP130 signaling inhibits cell viability/proliferation, glycolysis, and colony forming activity in human pancreatic cancer cells. Curr Cancer Drug Targets 2019; 19: 417-427.
[35] Li H, Liang Q and Wang L. Icaritin inhibits glioblastoma cell viability and glycolysis by blocking the IL-6/Stat3 pathway. J Cell Biochem 2018; [Epub ahead of print].
[36] Ota A, Hanamura I, Karnan S, Inaguma S, Takei N, Lam VQ, Mizuno S, Kanasugi J, Wahiduzzaman M, Rahman ML, Hyodo T, Konishi H, Tsuzuki S, Ikeda H, Takami A and Hosokawa Y. Novel interleukin-6 inducible gene PDZ-binding kinase promotes tumor growth of multiple myeloma cells. J Interferon Cytokine Res 2020; 40: 389-405.
[37] Zhu Y, Tchkonia T, Pirtskhalava T, Gower AC, Ding H, Giorgadze N, Palmer AK, Ikeno Y, Hubbard GB, Lenburg M, O'Hara SP, LaRusso NF, Miller JD, Roos CM, Verzosa GC, LeBrasseur NK, Wren JD, Farr JN, Khosla S, Stout MB, McGowan SJ, Fuhrmann-Stroissnigg H, Gurkar AU, Zhao J, Colangelo D, Dorronsoro A, Ling YY, Barghouthy AS, Navarro DC, Sano T, Robbins PD, Niedernhofer LJ and Kirkland JL. The Achilles' heel of senescent cells: from transcriptome to senolytic drugs. Aging Cell 2015; 14: 644-658.
[38] Chang J, Wang Y, Shao L, Laberge RM, Demaria M, Campisi J, Janakiraman K, Sharpless NE, Ding S, Feng W, Luo Y, Wang X, Aykin-Burns N, Krager K, Ponnappan U, Hauer-Jensen M, Meng A and Zhou D. Clearance of senescent cells by ABT263 rejuvenates aged hematopoietic stem cells in mice. Nat Med 2015; 22: 78-83.
[39] Bussian TJ, Aziz A, Meyer CF, Swenson BL, van Deursen JM and Baker DJ. Clearance of senescent glial cells prevents tau-dependent pathology and cognitive decline. Nature 2018; 562: 578-582.
[40] Baker DJ, Childs BG, Durik M, Wijers ME, Sieben CJ, Zhong J, Saltness RA, Jeganathan KB, Verzosa GC, Pezeshki A, Khazaie K, Miller JD and van Deursen JM. Naturally occurring p16(Ink4a)-positive cells shorten healthy lifespan. Nature 2016; 530: 184-189.